

# Experimental Verification and Simulation of Negative Index of Refraction Using Snell's Law

C.G. Parazzoli, R. B. Greegor, K. Li, B. E.C. Koltenbah, and M. Tanielian

## Abstract:

We report the results of a Snell's law experiment on a negative index of refraction material in free space from 12.6 to 13.2 GHz. Numerical simulations using Maxwell's equations solvers show good agreement with the experimental results, confirming the existence of negative index of refraction materials. The index of refraction is a function of frequency. At 12.6 GHz we measure and compute the real part of the index of refraction to be -1.05. The measurements and simulations of the electromagnetic field profiles were performed at distances of  $14 \lambda$  and  $28 \lambda$  from the sample; the fields were also computed at  $100 \lambda$ .

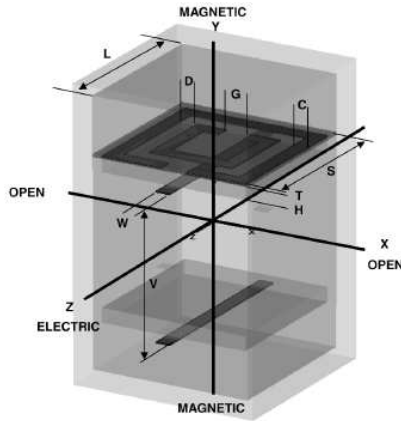


FIG. 1. Unit cell of the 90I HWD structure used in the numerical simulations. The direction of propagation of the electromagnetic field is along the  $x$  axis, the electric field is oriented along the  $z$  axis, and the magnetic field is along the  $y$  axis.  $C = 0.025$  cm,  $D = 0.030$  cm,  $G = 0.046$  cm,  $H = 0.0254$  cm,  $L = 0.33$  cm,  $S = 0.263$  cm,  $T = 17.0 \times 10^{-4}$  cm,  $W = 0.025$  cm, and  $V = 0.255$  cm.

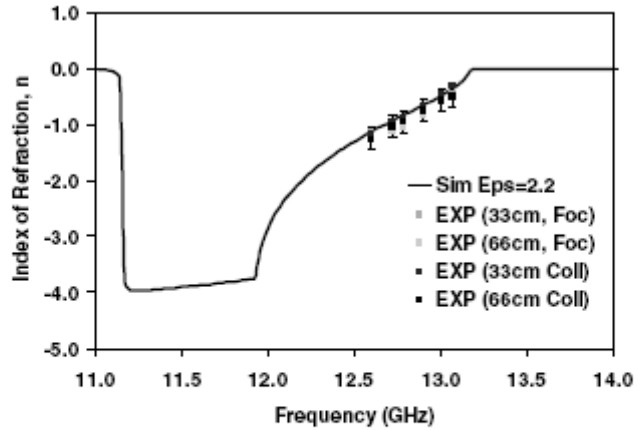


FIG. 7. Experimental and computed dispersion relation of the index of refraction for the 90I HWD structure with substrate  $\epsilon = 2.2$ . The experimental data were taken in both the focused and collimated beam setup at 33 and 66 cm from the wedge.

## Comment:

The effective index of refraction  $n$  versus frequency is computed numerically through inversion of the scattering coefficients. There is no mention about the inversion techniques used. Numerical simulations were performed using Lorentz dispersion for both permittivity and permeability, but no model parameters were indicated in order to validate the dispersion profile of  $n$ . Moreover the complex refractive index should exhibit a positive imaginary part.

# Wave Refraction in Negative-Index Media: Always Positive and Very Inhomogeneous

P.M. Valanju, R. M. Walser, and A. P. Valanju

Abstract:

We present the first treatment of the refraction of physical electromagnetic waves in newly developed negative index media (NIM), also known as left-handed media (LHM). The NIM dispersion relation implies that group fronts refract positively even when phase fronts refract negatively. This difference results in rapidly dispersing, very inhomogeneous waves. In fact, causality and finite signal speed always prevent negative wave signal (not phase) refraction. Earlier interpretations of phase refraction as “negative light refraction” and “light focusing by plane slabs” are therefore incorrect, and published NIM experiments can be explained without invoking negative signal refraction.

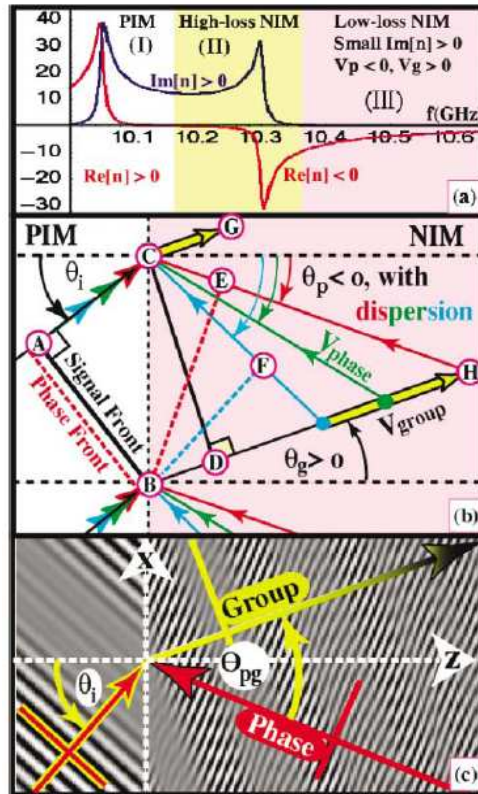


FIG. 1 (color). (a)  $n_p(\omega)$  for parameters in Ref. [4]. The low-loss NIM region (III) above two resonances has negative real parts of  $\epsilon$ ,  $\mu$ , and hence  $n_p$ , small imaginary parts, and  $\text{Re}[n_g] > 0$ . The anomalous dispersion region (II) is of less practical interest. (b) Negative and positive refractions of  $v_p$  and  $v_g$  in NIM. Three  $\omega$  components are shown. (c) Density plot of  $\text{Re}[E(t, x, z)]$  showing phase fronts (sharp bands), and group fronts (wider gray bands). Note signal dispersion at large  $z$  due to  $n_d$ , and large  $\theta_{pg}$  between phase and group fronts.

Comment:

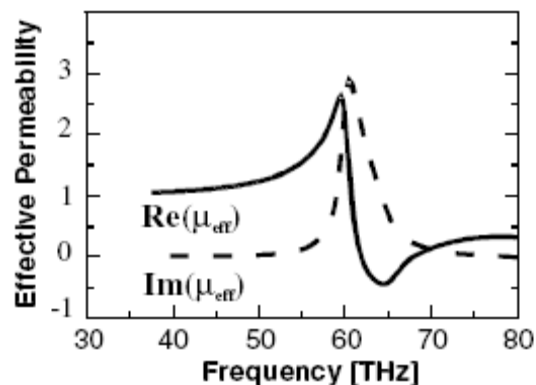
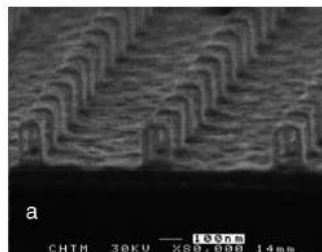
The effective index of refraction  $n$  versus frequency is calculated for a double dispersive medium. Both the permeability and permittivity have a Lorentz behavior (referring *R. A. Shelby, D. R. Smith, and S. Schultz, Science 77, 292 2001*). The shown profile is consistent with the proposed models.

# Midinfrared Resonant Magnetic Nanostructures Exhibiting a Negative Permeability

Shuang Zhang, Wenjun Fan, B. K. Minhas, Andrew Frauenglass, K. J. Malloy, and S. R. J. Brueck

## Abstract:

We experimentally demonstrate the first midinfrared (mid-IR) resonant magnetic nanostructures exhibiting a strong magnetic response corresponding to a negative permeability. This result is an important step toward the achievement of a negative refractive index in the IR. The possibility of extending negative permeability to higher frequencies is discussed; a structure with a negative effective permeability at a near-IR resonance frequency of 230 THz (1.3  $\mu\text{m}$ ) is proposed. The structure consists of an array of gold ‘‘staples’’ each with two outwardly splayed footings, separated from a thick continuous gold film by a ZnS dielectric layer.



## Comment:

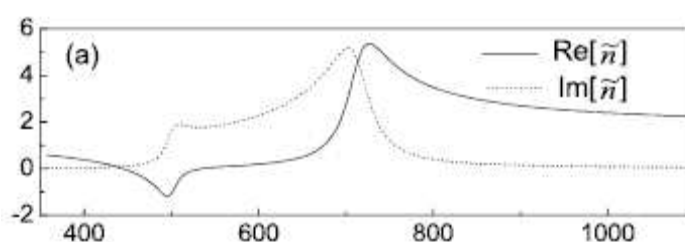
The proposed dispersion profile for the permeability is derived through inversion of the scattering coefficients (no mention about the specific technique or formulas). In the shown frequency range the effective parameters have a typical Lorentz behavior. The structures is clearly anisotropic, so the effective parameter characterization is consistently performed only for a TM polarized wave (that is when magnetic field is coupled with the loop of the staple).

# Negative Refraction at Optical Frequencies in Nonmagnetic Two-Component Molecular Media

Yi-Fan Chen, Peer Fischer, and Frank W. Wise

## Abstract:

There is significant motivation to develop media with negative refractive indices at optical frequencies, but efforts in this direction are hampered by the weakness of the magnetic response at such frequencies. We show theoretically that a nonmagnetic medium with two atomic or molecular constituents can exhibit a negative refractive index. A negative index is possible even when the real parts of both the permittivity and permeability are positive. This surprising result provides a route to isotropic negative-index media at optical frequencies.



## Comment:

This is a speculative work, in which the proposed effective refractive index is computed with reference to a Lorentz-oscillator approach for two atomic or molecular media. The permittivity is dispersive with a double resonance, while the permeability is constant (vacuum). The frequency profile of  $n$  appears to be consistent with the mathematical model showing no sign inversion for the imaginary part, but there is no verification of the proposed computed parameter.

# Saturation of the Magnetic Response of Split-Ring Resonators at Optical Frequencies

J. Zhou, Th. Koschny, M. Kafesaki, E. N. Economou, J. B. Pendry, and C. M. Soukoulis

## Abstract:

We investigate numerically the limits of the resonant magnetic response with a negative effective permeability  $\mu_{eff}$  for single-ring multicut split-ring resonator (SRR) designs up to optical frequencies. We find the breakdown of linear scaling due to the free electron kinetic energy for frequencies above  $\sim 100$  THz. Above the linear scaling regime, the resonance frequency saturates, while the amplitude of the resonant permeability decreases, ultimately ceasing to reach negative value. The highest resonance frequency at which  $\mu_{eff} < 0$  increases with the number of cuts in the SRR. A LC circuit model provides explanation of the numerical data.

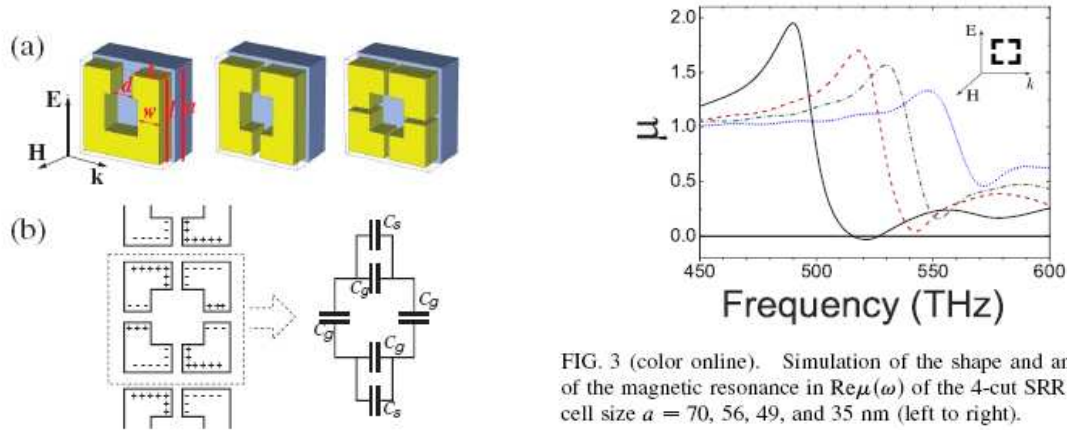


FIG. 3 (color online). Simulation of the shape and amplitude of the magnetic resonance in  $\text{Re}\mu(\omega)$  of the 4-cut SRR for unit cell size  $a = 70, 56, 49,$  and  $35$  nm (left to right).

## Comment:

As pointed out in the paper, the effective permeability  $\mu_{eff}(\omega)$  has been obtained from the simulated scattering data by employing the retrieval procedure presented in *D. R. Smith et al., Phys. Rev. E 71, 036617 (2005)*. The dispersion profile clearly shows a magnetic resonance in this specific frequency range with some changes in the slope at higher frequencies. There is no indication of the behavior of the imaginary part.

# Experimental Observation of Left-Handed Behavior in an Array of Standard Dielectric Resonators

Liang Peng, Lixin Ran, Hongsheng Chen, Haifei Zhang, Jin Au Kong and Tomasz M. Grzegorzczuk

## Abstract:

We demonstrate that by utilizing displacement currents in simple dielectric resonators instead of conduction currents in metallic split-ring resonators and by additionally exciting the proper modes, left-handed properties can be observed in an array of high dielectric resonators. Theoretical analysis and experimental measurements show that the modes, as well as the sub-wavelength resonance, play an important role in the origin of the left-handed properties. The proposed implementation of a left-handed metamaterial, based on a purely dielectric configuration, opens the possibility of realizing media at terahertz frequencies since scaling issues and losses, two major drawbacks of metal-based structures, are avoided.

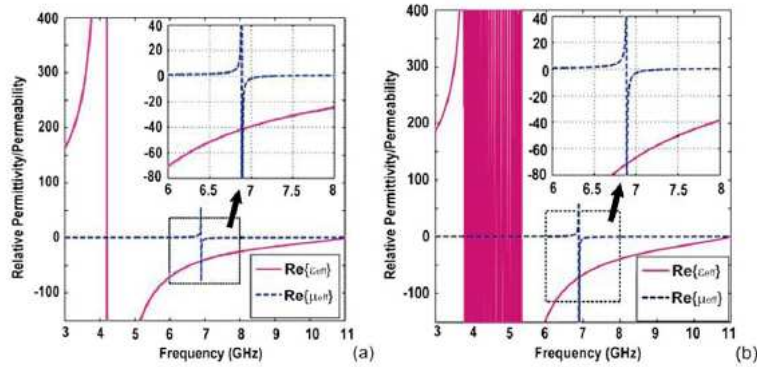


FIG. 2 (color online). Calculation of the effective relative permittivity  $\epsilon_{\text{eff},z}$  and the effective relative permeability  $\mu_{\text{eff},y}$  of the BST resonator array. (a) Periodic case and (b) random case. The black arrows point to the insets showing the enlarged regions enclosed by the dashed lines.

## Comment:

The configuration with a periodic array of scatterers shows a Lorentzian profile for both the permittivity and permeability (even if the complete dynamic is not entirely plotted). The setup for a randomly arranged array instead clearly has ambiguous values for the permeability, because the integral definition used for the effective parameters does not converge near the resonance frequency.

# Dielectric Metamaterials Based on Electric and Magnetic Resonances of Silicon Carbide Particles

Jon A. Schuller, Rashid Zia, Thomas Taubner, and Mark L. Brongersma

## Abstract:

Silicon carbide particles exhibit both electric and magnetic optical resonances, allowing unexplored dielectric metamaterial designs. Experimental extinction spectra and Mie theory calculations of single microscale rod-shaped particles reveal three observable midinfrared resonant modes. Two of the modes are degenerate, with a frequency that can be tuned according to a resonance condition derived within the Letter. The existence of both electric and magnetic resonances may enable a novel negative refractive index metamaterial design.

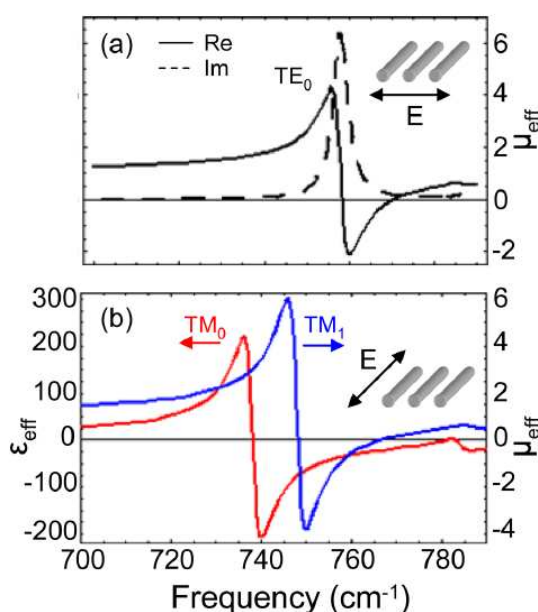


FIG. 4 (color online). (a) Calculated effective permeability for a normal incidence TE illuminated array of infinitely long 1.5  $\mu\text{m}$  diameter SiC rods. (b) Calculated permittivity (permeability) due to excitation of the zeroth (first) order TM mode. Imaginary components have been omitted for clarity.

## Comment:

The authors used a homogenization procedure that defines the effective permeability (permittivity) as the ratio of an average of the B (D) field over a unit cell face, and the H (E) field over a unit cell edge. They refer to *S. O'Brien and J. B. Pendry, J. Phys. Condens. Matter* **14**, 4035 (2002) and *D. R. Smith and J. B. Pendry, J. Opt. Soc. Am.* **B 23**, 391 (2006). The calculated dispersion profiles show a Lorentzian resonance (the zeroth order TM calculated parameters have multiple zero-crossing).

# Compact Dielectric Particles as a Building Block for Low-Loss Magnetic Metamaterials

Bogdan-Ioan Popa and Steven A. Cummer

## Abstract:

We characterize experimentally a compact dielectric particle that can be used to design very low-loss artificial electromagnetic materials (metamaterials). Focusing on magnetic media, we show that the particle can behave almost identically to the well-known split-ring resonators (SRRs) widely used in present designs, without suffering from the ohmic losses that can limit the applicability of SRRs especially at high frequencies. We experimentally compare qualitatively and quantitatively the dielectric particle with a typical split-ring resonator of the same size built on a low-loss dielectric substrate and show that at GHz frequencies the quality factor of the dielectric particle is more than 3 times bigger than that of its metallic counterpart. Low-loss and simple geometry are significant advantages compared to conventional metal SRRs.

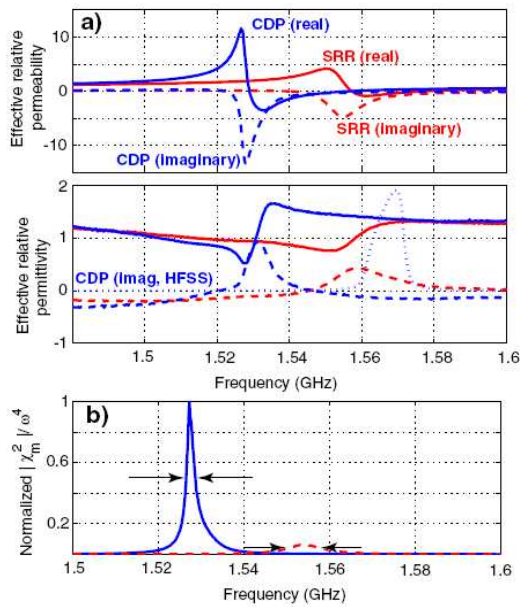


FIG. 2 (color online). (a) The retrieved real (solid) and imaginary (dashed) parts of the effective material parameters (top: permeability; bottom: permittivity) of the dielectric block (blue lines) and SRR (red lines). The small negative imaginary part of  $\epsilon$  is an experimental artifact that does not show in numerical simulations (blue dotted line). (b) The measured normalized  $|\chi_m^2|/\omega^4$  allows us to determine the quality factors of the two particles. We obtain  $Q = 509$  for the dielectric block (solid line), and  $Q = 141$  for the SRR (dashed line).

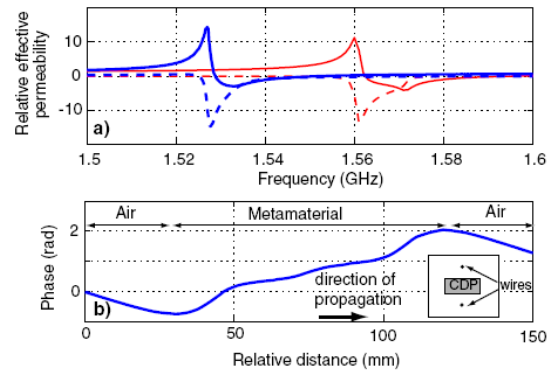


FIG. 3 (color online). (a) Comparison between the effective permeability real (solid) and imaginary (dashed) components retrieved in a numerical simulation (red) and experimentally (blue) for the CDP-based medium; (b) Phase distribution of the electric field at 1.53 GHz in front, inside, and behind a NIM made of CDPs and vertical wires. Inset: top view of unit cell.

## Comment:

The authors retrieve the effective parameters for both a SRR and a Compact Dielectric Particle (CDP) through the scattering coefficients inversion. In the numerical simulations the permeability function shows a quite clear Lorentzian profile for both the inclusions. The extracted permittivity is instead not consistent: the imaginary part has a sign inversion around the resonance frequency and the slope of the real part does not satisfy causality (the frequency derivatives of both  $\text{Re}(\epsilon)$  and  $\text{Re}(\mu)$  should be positive). For what concerns the experimental measurements, the sign of permeability imaginary part at lower frequencies appears to be inverted in the plotted dispersion.

# Experimental Demonstration of Near-Infrared Negative-Index Metamaterials

Shuang Zhang, Wenjun Fan,<sup>1</sup> N. C. Panoiu, K. J. Malloy,<sup>1</sup> R. M. Osgood, and S. R. J. Brueck

## Abstract:

Metal-based negative refractive-index materials have been extensively studied in the microwave region. However, negative-index metamaterials have not been realized at near-IR or visible frequencies due to difficulties of fabrication and to the generally poor optical properties of metals at these wavelengths. In this Letter, we report the first fabrication and experimental verification of a transversely structured metal-dielectric-metal multilayer exhibiting a negative refractive index around 2  $\mu\text{m}$ . Both the amplitude and the phase of the transmission and reflection were measured experimentally, and are in good agreement with a rigorous coupled wave analysis.

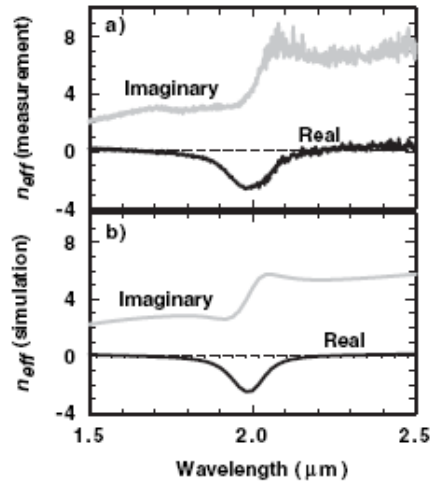


FIG. 5. The effective refractive index extracted from measurement (a) and from modeling (b) showing a resonance and a negative real part at  $\sim 2.0 \mu\text{m}$ .

## Comment:

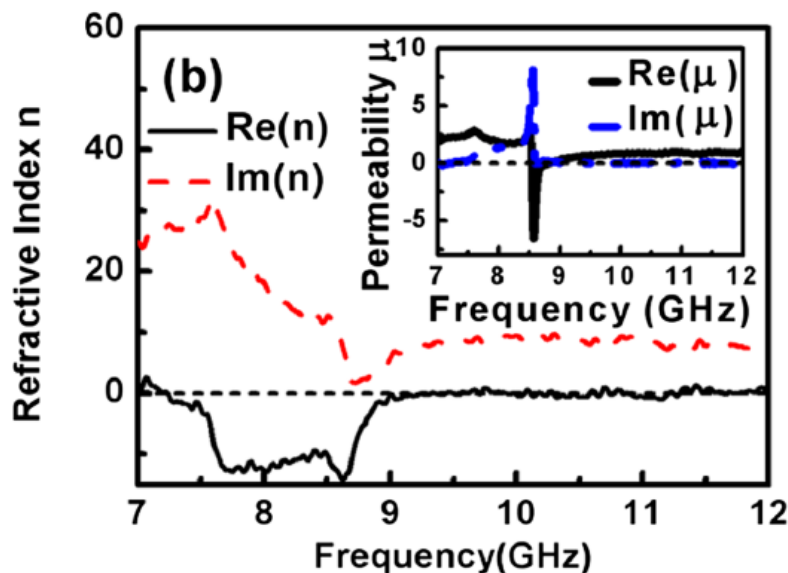
The effective index of refraction  $n$  versus wavelength is computed numerically through inversion of the scattering coefficients using standard Nicholson-Ross-Weir formulas. The imaginary part is always positive even if no dispersion profile for the effective constitutive parameters is reported.

# Experimental Demonstration of Isotropic Negative Permeability in a Three-Dimensional Dielectric Composite

Qian Zhao, Lei Kang, B. Du, H. Zhao, Q. Xie, X. Huang, B. Li, J. Zhou, and L. Li

## Abstract:

Isotropic negative permeability resulting from Mie resonance is demonstrated in a three-dimensional (3D) dielectric composite consisting of an array of dielectric cubes. A strong sub-wavelength magnetic resonance, corresponding to the first Mie resonance, was excited in dielectric cubes by electromagnetic wave. Negative permeability is verified in the magnetic resonance area via microwave measurement and the dispersion properties. The resonance relies on the size and permittivity of the cubes. It is promising for construction of novel isotropic 3D left-handed materials with a simple structure.



## Comment:

The effective index of refraction  $n$  versus frequency is measured through inversion of the scattering coefficients, computed with only one unit cell along the propagation direction. The retrieved effective permeability has a Lorentzian profile with a slope variation near the high-losses region at resonance. The medium is based on an array of dielectric cubic particles embedded in a non-magnetic matrix, so also a dispersive permittivity should be expected, as in Levin medium. However, no dispersion for the permeability is indicated, even if the sign of the imaginary part of both  $n$  and  $\mu$  appears to be consistent.

# LongWave–ShortWave Resonance in Nonlinear Negative Refractive Index Media

Aref Chowdhury and John A. Tataronis

Abstract:

We show that long wave–short wave resonance can be achieved in a second-order nonlinear negative refractive index medium when the short wave lies on the negative index branch. With the medium exhibiting a second-order nonlinear susceptibility, a number of nonlinear phenomena such as solitary waves, paired solitons, and periodic wave trains are possible or enhanced through the cascaded second order effect. Potential applications include the generation of terahertz waves from optical pulses.

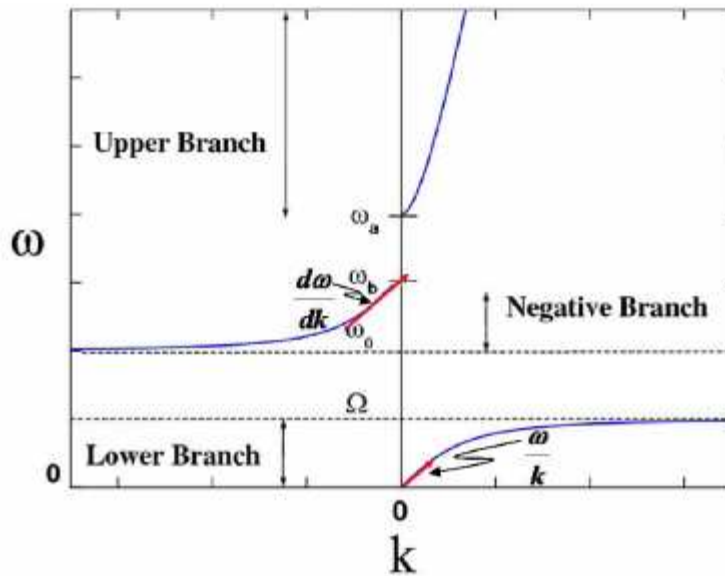


FIG. 1 (color online). Depiction of LWSW resonance on a dispersion diagram  $\omega$  vs  $k$  based on Eq. (3) with  $\Omega < \omega_0 < \omega_b < \omega_a$ . The parallel lines show the matching of the group and phase velocities on the negative and lower branches, respectively.

Comment:

This is a purely theoretical study. The dispersion profile for both the permittivity and the permeability is set analytically. The sign of  $k$  is chosen by causality.

# Negative Refraction in Ferromagnet-Superconductor Superlattices

A. Pimenov, A. Loidl, P. Przyslupski, and B. Dabrowski

Abstract:

Negative refraction, which reverses many fundamental aspects of classical optics, can be obtained in systems with negative magnetic permeability and negative dielectric permittivity. This Letter documents an experimental realization of negative refraction at millimeter waves, finite magnetic fields, and cryogenic temperatures utilizing a multilayer stack of ferromagnetic and superconducting thin films. In the present case the superconducting  $\text{YBa}_2\text{Cu}_3\text{O}_7$  layers provide negative permittivity while negative permeability is achieved via ferromagnetic  $(\text{La:Sr})\text{MnO}_3$  layers for frequencies and magnetic fields close to the ferromagnetic resonance. In these superlattices the refractive index can be switched between positive and negative regions using external magnetic field as tuning parameter.

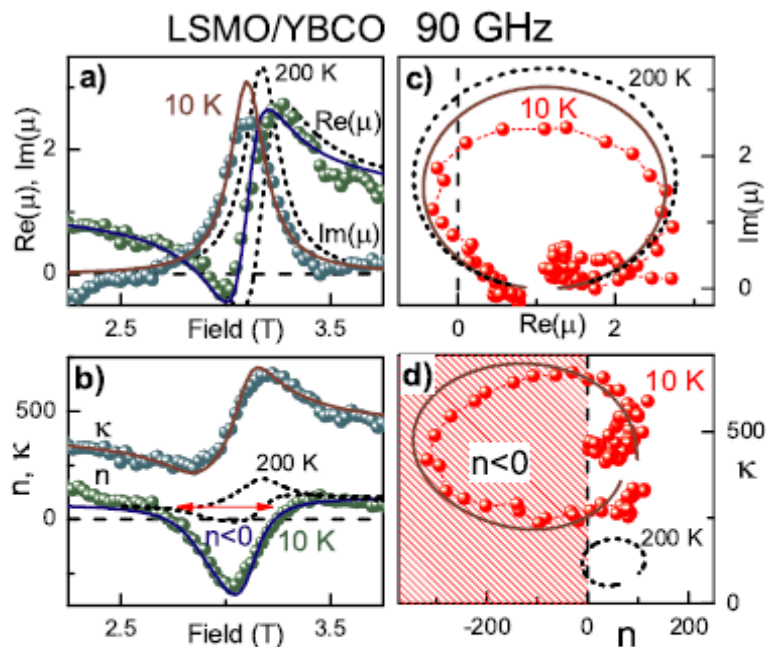


FIG. 3 (color online). Magnetic permeability of LSMO/YBCO superlattices at  $T = 10$  K as function of magnetic field (a) and replotted in the complex plane (c). The complex refractive index as field dependence (b) and in the complex plane (d). The shaded area corresponds to the region with negative real part of refractive index. The results for  $T = 200$  K are given for comparison. In all frames the symbols correspond to experimental data; lines represent the Lorentz model for the FMR line.

Comment:

This is an experimental study. The magnetic permeability is given analytically as a function of the magnetic field intensity, while experimentally it is given as a function of the temperature. No dispersion relations are clearly given.

# Simulations of Ferrite-Dielectric-Wire Composite Negative Index Materials

Frederic J. Rachford, Vincent G. Harris, Carmine Vittoria, Douglas N. Armstead

## Abstract:

We perform extensive finite difference time domain simulations of ferrite based negative index of refraction composites. A wire grid is employed to provide negative permittivity. The ferrite and wire grid interact to provide both negative and positive index of refraction transmission peaks in the vicinity of the ferrite resonance. Notwithstanding the extreme anisotropy in the index of refraction of the composite, negative refraction is seen at the composite air interface allowing the construction of a focusing concave lens with a magnetically tunable focal length.

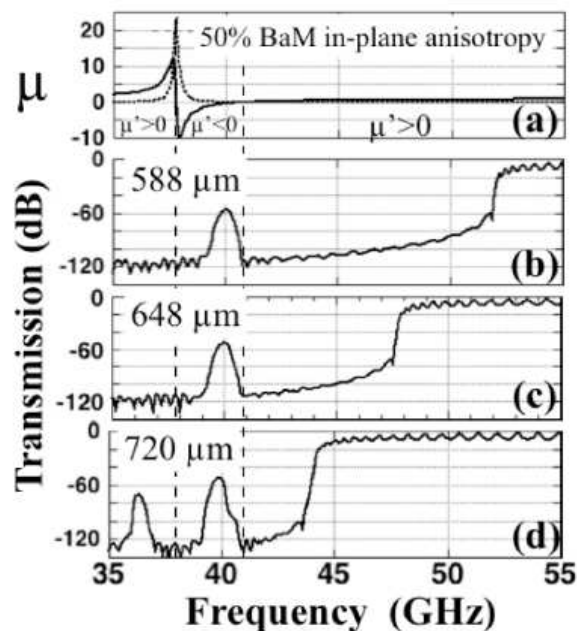


FIG. 2. A series of transmission spectra through 39 unit thickness of the BaM-Mylar-wire composite varying the spacing of the square wire grid. As the spacing increases the high pass cutoff is reduced in frequency. As the cutoff approaches the BaM resonance a second peak appears below the FMR frequency (d). The complex relative permeability of BaM at 50% loading is shown for reference (a).

## Comment:

This is a theoretical study. The dispersion curve given for the permeability exhibits a typical Lorentz profile.

# Tunable Negative Refraction without Absorption via Electromagnetically Induced Chirality

Jürgen Kästel, Michael Fleischhauer, Susanne F. Yelin and Ronald L. Walsworth

## Abstract:

We show that negative refraction with minimal absorption can be obtained by means of quantum interference effects similar to electromagnetically induced transparency (EIT). Coupling a magnetic dipole transition coherently with an electric dipole transition leads to electromagnetically induced chirality, which can provide negative refraction without requiring negative permeability and also suppress absorption. This technique allows negative refraction in the optical regime at densities where the magnetic susceptibility is still small and with refraction/absorption ratios that are orders of magnitude larger than those achievable previously. Furthermore, the refractive index can be fine-tuned, which is essential for practical realization of subdiffraction-limit imaging. As with EIT, electromagnetically induced chirality should be applicable to a wide range of systems.

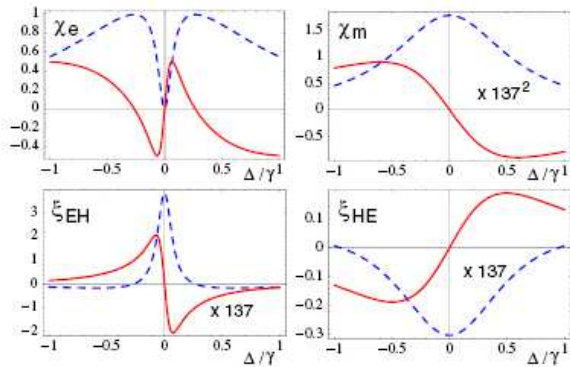


FIG. 2 (color online). Real (solid lines) and imaginary (dashed lines) parts of the electric ( $\chi_e$ ) and magnetic ( $\chi_m$ ) susceptibilities as well as the chirality parameters ( $\xi_{HE}$ ,  $\xi_{EH}$ ) without local-field corrections in arbitrary but the same units, as a function of the probe field detuning  $\Delta$  relative to the radiative decay rate  $\gamma_3$  from level  $|3\rangle$ .

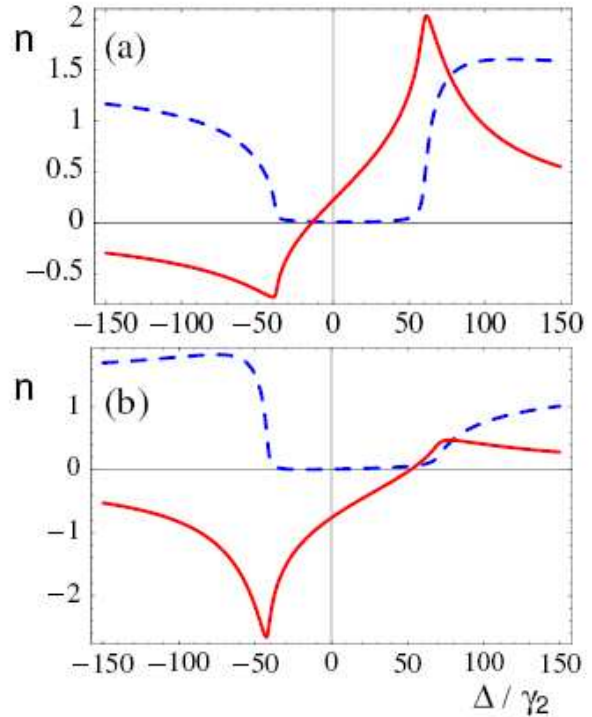


FIG. 3 (color online). Real (solid lines) and imaginary (dashed lines) parts of the refractive index as a function of the probe field detuning  $\Delta$  relative to the radiative decay rate  $\gamma_2$  from level  $|2\rangle$ , for a density of (a)  $N = 5 \times 10^{16} \text{ cm}^{-3}$  and (b)  $N = 5 \times 10^{17} \text{ cm}^{-3}$ .

## Comment:

The given dispersion profile for the electric susceptibility is not consistent: the slope of the real part is inverted (always negative) and the profile for the imaginary part is unusual as it exhibits a minimum at the resonance frequency.

# Negative Refraction Observed in a Metallic Ferromagnet in the Gigahertz Frequency Range

A. Pimenov, A. Loidl, K. Gehrke, V. Moshnyaga, and K. Samwer

## Abstract:

It is generally believed that nature does not provide materials with negative refraction. Here we demonstrate experimentally that such materials do exist at least at GHz frequencies: ferromagnetic metals reveal a negative refraction index close to the frequency of the ferromagnetic resonance. The experimental realization utilizes a colossal magnetoresistance manganite  $\text{La}_{2/3}\text{Ca}_{1/3}\text{MnO}_3$  as an example. In this material the negative refractive index can be achieved even at room temperature using external magnetic fields.

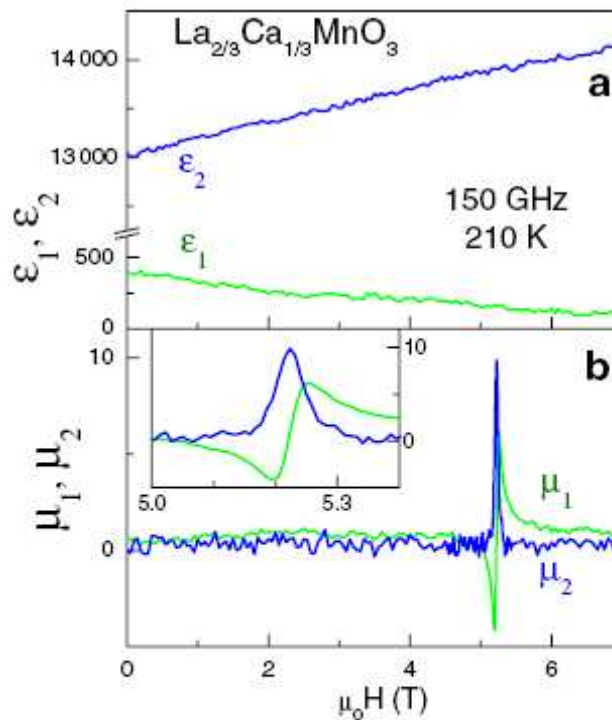


FIG. 3 (color online). Magnetic field-dependence of the dielectric permittivity (a) and magnetic permeability (b) of LCMO at  $\nu = 150$  GHz and  $T = 210$  K. Green curves—real parts, blue curves—imaginary parts. The inset shows the magnetic permeability in the vicinity of the resonance field.

## Comment:

This is an experimental study. The dispersion curve of the permeability is not consistent, exhibiting an inverted-slope Lorentz profile for the real part.

# Design of an Artificial Three-Dimensional Composite Metamaterial with Magnetic Resonances

Carsten Rockstuhl, Falk Lederer, Christoph Etrich, Thomas Pertsch and Toralf Scharf

We propose an artificial three-dimensional material that exhibits a strong resonance in the effective permeability in the visible spectral domain. This material may be implemented in a two-step procedure. First, a metamaterial made of densely packed metallic nanoparticles is fabricated that shows a Lorentz type resonance in the permittivity at the collective plasmon frequency. Second, spheres are formed out of this material and arranged in a cubic lattice. This meta-metamaterial exhibits a strong resonance in the permeability which is caused by a Mie resonance associated with the magnetic mode of a single metamaterial sphere. Realization of this material based on self-organization in liquid crystals and the limitations of the approach are discussed.

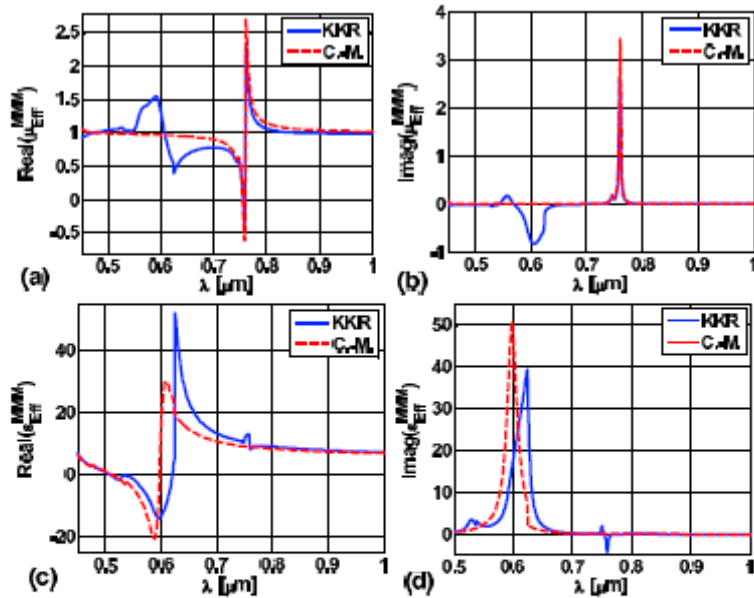


FIG. 3 (color online). Effective material parameters of a MMM that consists of spheres ( $R^{\text{MM}} = 22.5$  nm) arranged in a cubic lattice ( $a^{\text{MM}} = 50$  nm). The material properties of the spheres are those shown in Fig. 2 with a period of  $a = 6$  nm. Calculations were performed with the KKR method and effective medium theory.

## Comment:

This is an experimental study. The given dispersion profiles are consistent: the first derivative of the extracted dispersive profile is always negative. The dispersive profiles calculated with the KKR method exhibit an additional resonance, but the imaginary part exhibits both positive and negative values resulting not completely consistent.

# Experimental Demonstration of Electromagnetic Tunneling Through an Epsilon-Near-Zero Metamaterial at Microwave Frequencies

Ruopeng Liu, Qiang Cheng, Thomas Hand and Jack J. Mock, Tie Jun Cui

Silveirinha and Engheta have recently proposed that electromagnetic waves can tunnel through a material with an electric permittivity near zero (ENZ). An ENZ material of arbitrary geometry can thus serve as a perfect coupler between incoming and outgoing waveguides with identical cross-sectional area, so long as one dimension of the ENZ is electrically small. In this Letter we present an experimental demonstration of microwave tunneling between two planar waveguides separated by a thin ENZ channel. The ENZ channel consists of a planar waveguide in which complementary split ring resonators are patterned on the lower surface. A tunneling passband is found in transmission measurements, while a two dimensional spatial map of the electric field distribution reveals a uniform phase variation across the channel—both measurements in agreement with theory and numerical simulations.

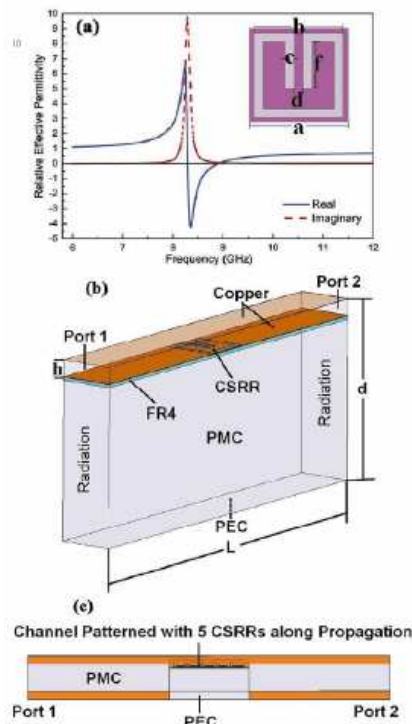


FIG. 2 (color online). Retrieval results, dimensions of CSRRs, and simulation setup. (a) Extracted permittivity and CSRRs' dimensions, in which  $a = 3.333$  mm,  $b = 3$  mm,  $c = d = 0.3$  mm, and  $f = 1.667$  mm. (b) Simulation configuration for CSRR unit cell.  $d = 11$  mm,  $h = 1$  mm, and  $L = 23.333$  mm. (c) Configuration of tunneling effect simulation.

## Comment:

This is an experimental study. The dispersion of the permittivity exhibits a typical Lorentz profile.

# Dynamical Electric and Magnetic Metamaterial Response at Terahertz Frequencies

W. J. Padilla, A. J. Taylor, C. Highstrete, Mark Lee and R. D. Averitt

Utilizing terahertz time domain spectroscopy, we have characterized the electromagnetic response of a planar array of split ring resonators (SRRs) fabricated upon a high resistivity GaAs substrate. The measured frequency dependent magnetic and electric resonances are in excellent agreement with theory and simulation. For two polarizations, the SRRs yield a negative electric response ( $\epsilon < 0$ ). We demonstrate, for the first time, dynamical control of the electrical response of the SRRs through photoexcitation of free carriers in the substrate. An excited carrier density of  $4 \times 10^{16} \text{ cm}^{-3}$  is sufficient to short the gap of the SRRs, thereby turning off the electric resonance, demonstrating the potential of such structures as terahertz switches. Because of the universality of metamaterial response over many decades of frequency, these results have implications for other regions of the electromagnetic spectrum.

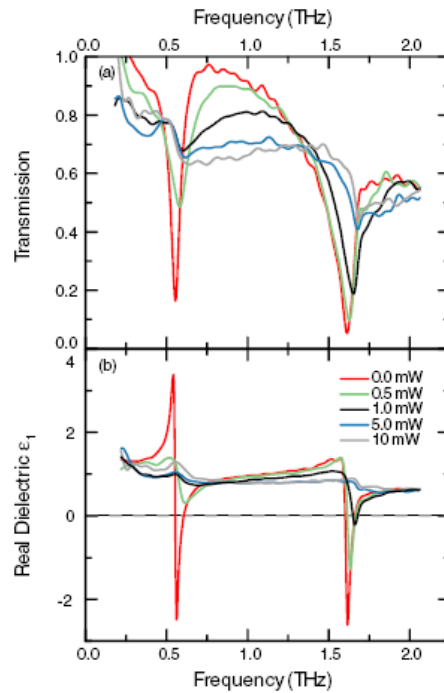


FIG. 3 (color online). (a) Transmission spectra as a function of photodoping fluence for the electric resonance of the SRRs. The polarization of the incident EM wave is as shown in Fig. 1(c). As the power is increased, the first mode is shorted out and the overall transmission decreases. At higher powers, the second mode can also be seen to die off. (b) Corresponding change of the real dielectric constant  $\epsilon_1(\omega)$  of the SRRs as a function of power.

## Comment:

This is an experimental study. The dispersion curve of the permeability is the superimposition of two different Lorentz profile. The imaginary part is not given.

# Negative Refractive Index in Left-Handed Materials

David R. Smith\* and Norman Kroll

The real part of the refractive index  $n(\omega)$  of a nearly transparent and passive medium is usually taken to have only positive values. Through an analysis of a current source radiating into a 1D “left-handed” material (LHM)—where the permittivity and permeability are simultaneously less than zero—we determine the analytic structure of  $n(\omega)$ , demonstrating frequency regions where the sign of  $\text{Re}[n(\omega)]$  must, in fact, be negative. The regime of negative index, made relevant by a recent demonstration of an effective LHM, leads to unusual electromagnetic wave propagation and merits further exploration.

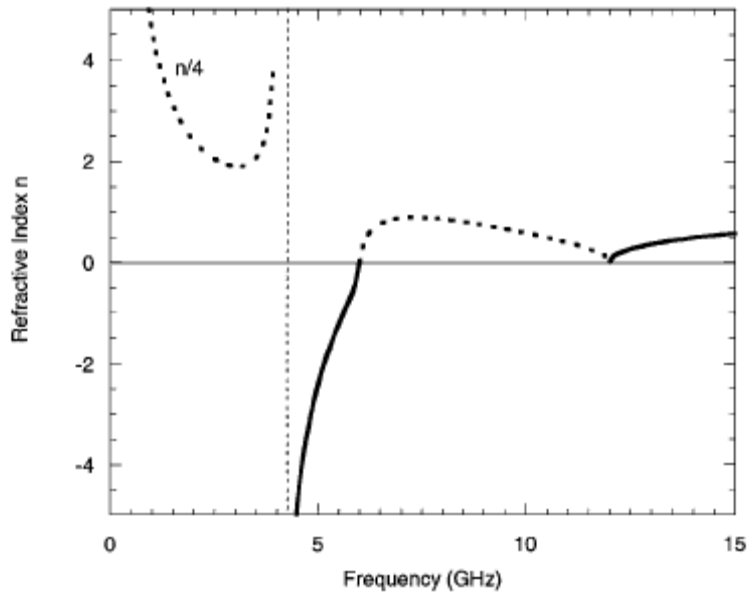


FIG. 4. Real (solid) and imaginary (dashed) branches of  $n(\omega)$  versus frequency. The region where  $n(\omega)$  is negative occurs when the permeability and permittivity are both negative. For this example, and to be somewhat compatible with the experimental values obtained in [2], we have chosen  $\omega_p = 12.0$  GHz,  $\omega_b = 6.0$  GHz, and  $\omega_0 = 4.0$  GHz.

## Comment:

This is a theoretical study. The dispersion model imposed for the electric permittivity is a standard Drude model, while for the magnetic permeability a Lorenz model is used.

# Negative Magnetic Permeability in the Visible Light Region

Atsushi Ishikawa Takuo Tanaka and Satoshi Kawata

Negative magnetic permeability of single split-ring resonators (SSRRs) is theoretically investigated in the visible light region. To describe the conduction characteristics of metal in the visible range, we develop the internal impedance formula completely. In our calculations, we determine the magnetic responses of the SSRR accurately. Based on our investigations, we also demonstrate the negative  $\mu$  of the silver SSRR array in the visible light region.

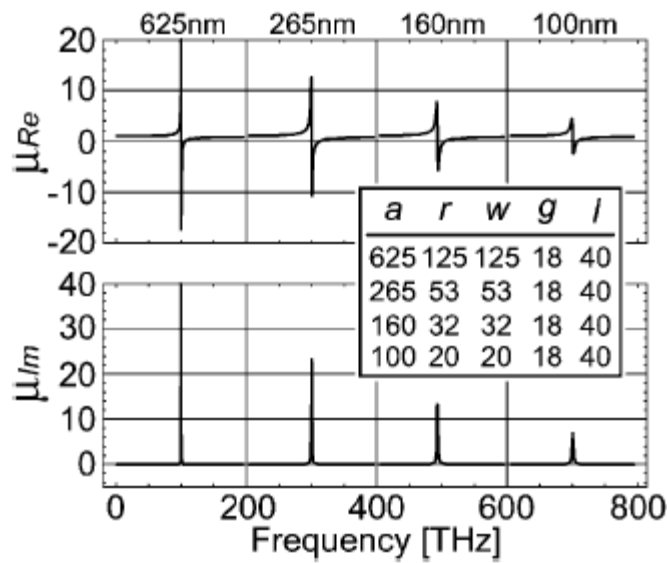


FIG. 3. Real and imaginary parts of the effective permeability of the silver SSRRs in the host material ( $\epsilon_r = 2.25$ ) as a function of the SSRRs' dimensions. The labeling in each case indicates the unit-cell dimension  $a$ . The inset shows the corresponding dimensions of the SSRR in nanometers.

## Comment:

This is a theoretical study. The dispersion curve of the permeability is the superimposition of four Lorentz profiles. The imaginary part is always positive.

# Composite Medium with Simultaneously Negative Permeability and Permittivity

D. R. Smith, Willie J. Padilla, D. C. Vier, S. C. Nemat-Nasser, and S. Schultz

Negative magnetic permeability of single split-ring resonators (SSRRs) is theoretically investigated in the visible light region. To describe the conduction characteristics of metal in the visible range, we develop the internal impedance formula completely. In our calculations, we determine the magnetic responses of the SSRR accurately. Based on our investigations, we also demonstrate the negative  $\mu$  of the silver SSRR array in the visible light region.

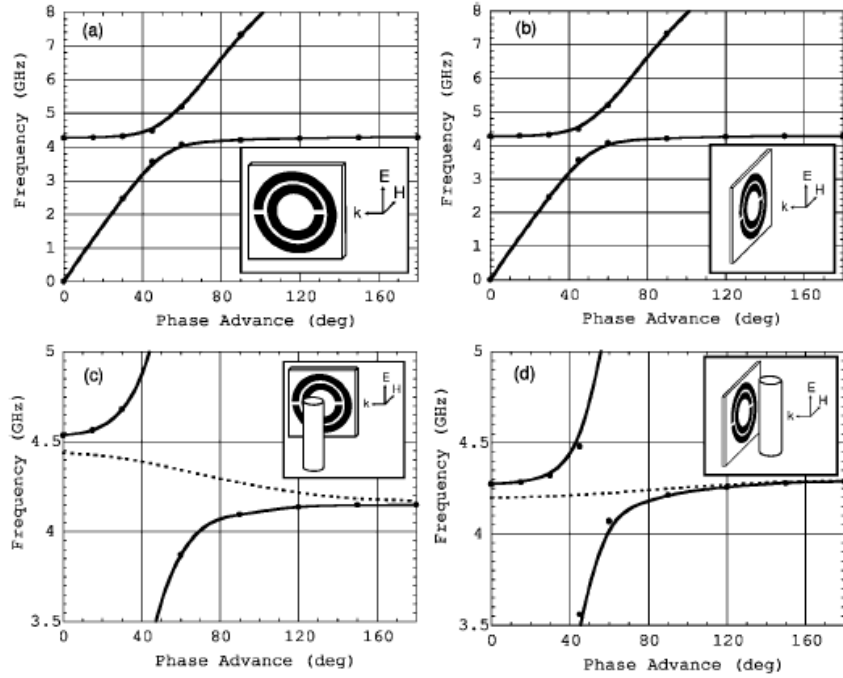


FIG. 2. (a) Dispersion curve for the parallel polarization  $H_{\parallel}$ . The lines with the solid circles correspond to the split ring resonators only. The inset shows the orientation of the split ring with respect to the incident radiation. The horizontal axis is the phase advance per unit cell, or  $kd$ , where  $k$  is the wave number. (b) Dispersion curve for the perpendicular polarization  $H_{\perp}$ . The lines with the solid circles correspond to the split ring resonators only. The inset shows the orientation of the split ring with respect to the incident radiation. (c) Expanded view of the dispersion curve shown in (a). The dashed line corresponds to the split ring resonators with wires placed uniformly between split rings. (d) Expanded view of the dispersion curve shown in (b). The dashed line corresponds to the split ring resonators with wires placed uniformly between split rings. The insets to (c) and (d) show the orientations of the split rings with respect to the wires.

## Comment:

Only dispersion diagram is given, but it is not clear what kind of material dispersion the proposed SRR medium exhibits.

# Nonlinear Properties of Left-Handed Metamaterials

Alexander A. Zharov, Ilya V. Shadrivov, and Yuri S. Kivshar

We analyze the properties of microstructured materials with negative refraction, the so-called *lefthanded metamaterials*. We consider a two-dimensional periodic structure created by arrays of wires and split-ring resonators embedded into a nonlinear dielectric, and calculate the effective nonlinear electric permittivity and magnetic permeability. We demonstrate that the hysteresis-type dependence of the magnetic permeability on the field intensity allows changing the material properties from left to right-handed and back. These effects can be treated as *the second-order phase transitions* in the transmission properties induced by the variation of an external field.

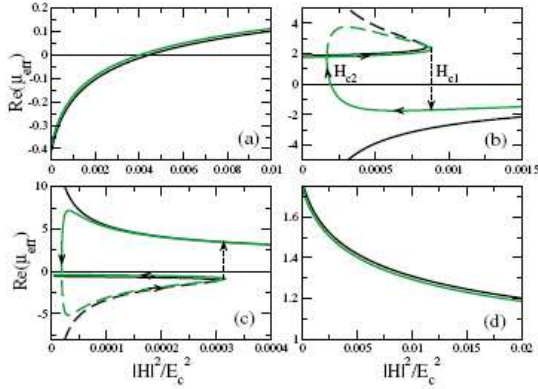


FIG. 2 (color online). The real part of the effective magnetic permeability versus intensity of the magnetic field: (a)  $\Omega > 1$ ,  $\alpha = 1$ ; (b)  $\Omega < 1$ ,  $\alpha = 1$ ; (c)  $\Omega > 1$ ,  $\alpha = -1$ ; (d)  $\Omega < 1$ ,  $\alpha = -1$ . Black: the lossless case ( $\gamma = 0$ ); grey: the lossy case ( $\gamma = 0.05$ ). The dashed curves show unstable branches.

## Comment:

The dispersion of  $\mu$  and  $\epsilon$  are imposed analytically. The Drude model is set for the electric permittivity and the Lorentz model is set for the magnetic permeability.

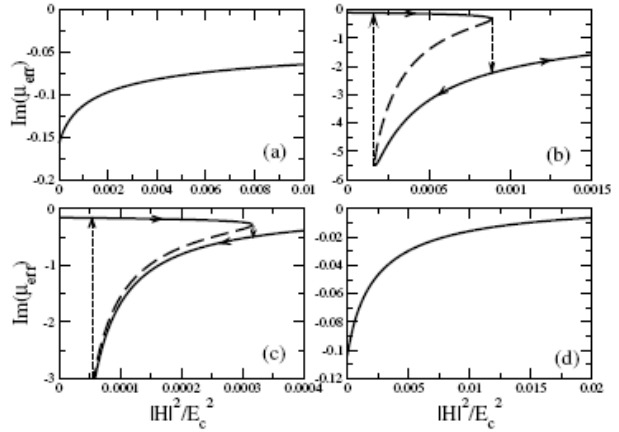


FIG. 3. The imaginary part of the effective magnetic permeability versus intensity of the magnetic field for  $\gamma = 0.05$ : (a)  $\Omega > 1$ ,  $\alpha = 1$ ; (b)  $\Omega < 1$ ,  $\alpha = 1$ ; (c)  $\Omega > 1$ ,  $\alpha = -1$ ; (d)  $\Omega < 1$ ,  $\alpha = -1$ . The dashed curves show unstable branches.

# Causality-Based Criteria for a Negative Refractive Index Must Be Used With Care

P. Kinsler and M.W. McCall

Using the principle of causality as expressed in the Kramers-Kronig relations, we derive a generalized criterion for a negative refractive index that admits imperfect transparency at an observation frequency  $\omega$ . It also allows us to relate the global properties of the loss (i.e., its frequency response) to its local behavior at  $\omega$ . However, causality-based criteria rely on the group velocity, not the Poynting vector. Since the two are not equivalent, we provide some simple examples to compare the two criteria.

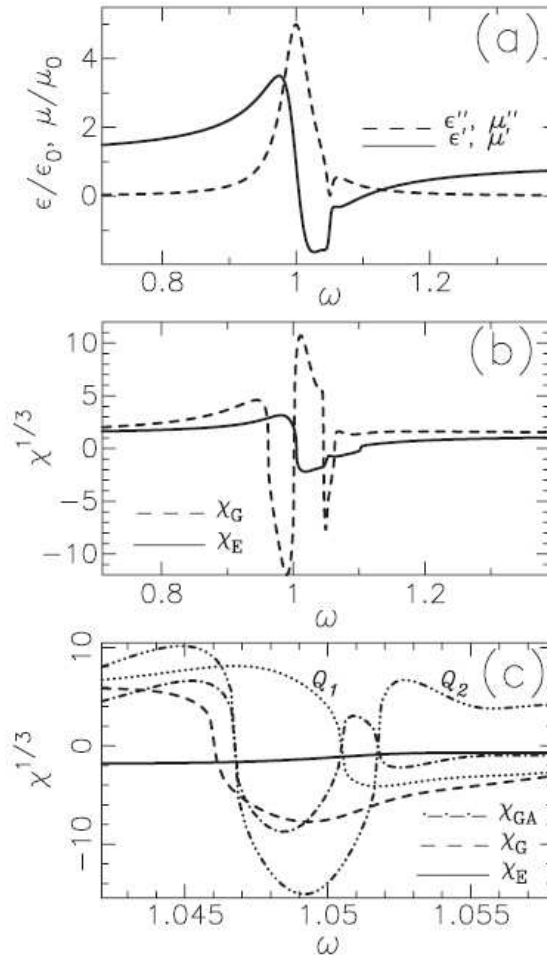


FIG. 2. A system exhibiting narrow band NRI. It combines a lossy resonance at  $\omega_1 = 1$  (with  $\gamma_1 = 0.05$ ,  $\sigma_1 = -5$ ) and an active one at  $\omega_2 = 1.05$  (with  $\gamma_2 = 0.01$  and  $\sigma_2 = 1.02$ ). (a) The real parts and imaginary parts of  $\epsilon$  and  $\mu$ . (b) Comparison of the NPVE ( $\chi_E$ ) and NPVG ( $\chi_G$ ) criteria. (c) Expanded view around  $\omega_2 = 1.05$ , showing also the NPVG approximation from Eq. (6) (labeled  $\chi_{GA}$ ), and  $Q_1$  and  $Q_2$ .

## Comment:

This is a theoretical study. The dispersion curve given for the permeability is a Lorentz-like profile. The imaginary part is always positive. The first derivative of the real part is always positive outside the resonance region.